Ocean Science Journal, 40(1), 25-44(2005)

Review

Ocean Science Journal

http://library.kordi.re.kr/OceanScience/

Long-term and Real-time Monitoring System of the East/Japan Sea

Kuh Kim*, Yun Bae Kim, Jong Jin Park, SungHyun Nam, Kyung-Ae Park, and Kyung-Il Chang

School of the Earth and Environmental Sciences, College of Natural Sciences, Seoul National University, Seoul 151-747, Korea

Received 21 February 2005; Revised 11 March 2005; Accepted 19 March 2005

Abstract – Long-term, continuous, and real-time ocean monitoring has been undertaken in order to evaluate various oceanographic phenomena and processes in the East/Japan Sea. Recent technical advances combined with our concerted efforts have allowed us to establish a real-time monitoring system and to accumulate considerable knowledge on what has been taking place in water properties, current systems, and circulation in the East Sea. We have obtained information on volume transport across the Korea Strait through cable voltage measurements and continuous temperature and salinity profile data from ARGO floats placed throughout entire East Sea since 1997. These ARGO float data have been utilized to estimate deep current, inertial kinetic energy, and changes in water mass, especially in the northern East Sea. We have also developed the East Sea Real-time Ocean Buoy (ESROB) in coastal regions and made continual improvements till it has evolved into the most up-to-date and effective monitoring system as a result of remarkable technical progress in data communication systems. Atmospheric and oceanic measurements by ESROB have contributed to the recognition of coastal wind variability, current fluctuations, and internal waves near and off the eastern coast of Korea. Long-term current meter moorings have been in operation since 1996 between Ulleungdo and Dokdo to monitor the interbasin deep water exchanges between the Japanese and Ulleung Basins. In addition, remotely sensed satellite data could facilitate the investigation of atmospheric and oceanic surface conditions such as sea surface temperature (SST), sea surface height, near-surface winds, oceanic color, surface roughness, and so on. These satellite data revealed surface frontal structures with a fairly good spatial resolution, seasonal cycle of SST, atmospheric wind forcing, geostrophic current anomalies, and biogeochemical processes associated with physical forcing and processes. Since the East Sea has been recognized as a natural laboratory for global oceanic changes and a clue to abrupt climate change, we aim at constructing a 4-D continuous real-time monitoring system, over a decade at least, using the most advanced techniques to understand a variety of oceanic processes in the East Sea.

Key words – real-time monitoring, cable voltage measurement, ARGO float, ESROB, current meter mooring, the East Sea, satellite data.

*Corresponding author. E-mail: kuhkim@ocean.snu.ac.kr

1. Introduction

The East Sea is a semi-enclosed marginal sea of the northwest Pacific, but it has phenomena and circulation patterns similar to those found in the open ocean (Kim *et al.* 2001). Its size is relatively small, but its depth is comparable to that of the open ocean; the Japan Basin (JB) in the north is nearly 4000 m deep, the Ulleung Basin (UB) and the Yamato Basin in the south are deeper than 2000 m. The water exchange of the East Sea with the North Pacific Ocean is limited to the upper layer through four channels; Korea, Tsugaru, Soya, and Tatarsky Straits. The wide range of open ocean processes evident in the East Sea together with its relatively small size and weak coupling with the open ocean are of particular interest to the oceanographic community; it provides a natural laboratory for studying oceanic processes both observationally and numerically.

In light of this, extensive research on its circulation, currents, water mass and hydrography, eddies, fronts in the East Sea have been performed until now. Essential to these studies is the collection of as many in-situ observational data as possible. During the past decade, we have conducted numerous cruises in order to collect a large amount of data of high accuracy through domestic and/or international programs like Circulation Research of the East Asian Marginal Seas (CREAMS). One of the biggest problems in the cruise measurement is that severe weather conditions often prevent us from collecting the physical and chemical data, especially in winter during the periods of Siberian cold-air outbreak. One of the other problems is that there is an inaccessible region particularly in the seas off North Korea. All of these difficulties have led us to devise an unmanned real-time monitoring system for the East Sea utilizing cable voltage measurement across the Korea Strait, satellite-tracking of the surface and subsurface drifters, a current meter mooring system, an atmospheric

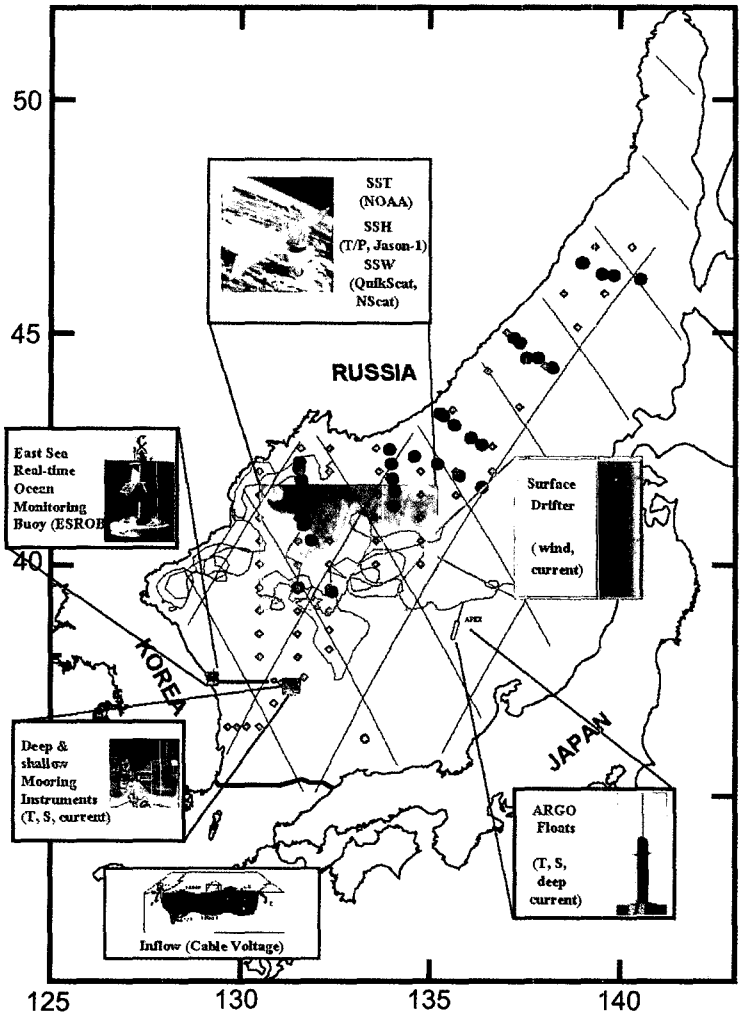

Fig. 1. Configuration of real-time monitoring system in the East Sea.

and oceanic buoy system off the coastal area, and a variety of satellites as shown in Fig. 1. Those systems have transmitted a number of data measurements mostly on a real-time basis to our laboratory.

Recent technical advances combined with our extensive efforts to develop a real-time ocean monitoring system have enabled us to accumulate considerable knowledge on what is/has been happening in water properties, current systems, and circulation in the East Sea. In the following, we briefly introduce instrumentation for the system and on our up-to-date research results based on the monitoring data. Section 2 describes a methodology of cable voltage measurements to calculate transport and some other results, and Section 3 covers quality control processes of ARGO float data and their applications to deep current estimation and inertial energy in the ocean. Section 4 introduces the history of how we have developed and operated our buoy systems moored in coastal regions, along with major research results using the data. In section 5, we describe the current meter moorings and new findings in the southwestern East Sea. Section 6 describes our attempts to optimize satellite data on the East Sea and presents some applications of the data. Each section also presents a brief ongoing and future plan for continuous real-time monitoring of the East Sea.

2. Monitoring Volume Transport through Measurement of Cable Voltage across the Korea Strait

It has been known that the Tsushima Warm Current brings warm and saline water into the East Sea through the Korea Strait, which is shallower than 200 m. Numerical experiments show that the variability of the circulation in the East Sea depends largely on the transport variation through the Korea Straits (Holloway *et al.* 1995; Kim and Yoon 1999). Therefore, continuous

monitoring of the transport in the Korea Strait is essential for understanding the circulation of the East Sea. Since February 1997, currents in the Korea Strait have been measured by a vessel-mounted Acoustic Doppler Current Profiler (ADCP) along a track between Busan, Korea and Hakata, Japan, six times per week (Takikawa *et al.* 1999). The U.S. Naval Research Laboratory (NRL) also deployed 12 ADCPs housed in trawl resistant bottom-mounts along two lines in the Korea Strait during May 1999 to March 2000 (Teague *et al.* 2002). However, it is difficult to monitor the flow through the Korea Strait using such a mooring system because of economic considerations and intense fishing activities in the Korea Strait. In the following, our methodology to exploit an abandoned submarine cable to monitor the transport and major results are summarized.

Methodology

According to Faraday's law, when seawater possessing electric conductivity flows through a strait under the geomagnetic field, potential electric differences are induced that are related to the volume transport through the strait (Sandford and Flick 1975). The same technique is applied to the Korea Strait using an abandoned submarine telephone cable between Busan, Korea and Hamada, Japan in order to monitor the volume transport through the Korea Strait (Kim *et al.* 2004b; Lyu *et al.* 2002a; Lyu *et al.* 2002b ; Lyu *et al.* 2003). Since March 1998, the voltage has been measured at the Busan Submarine Cable Relay Station, which is in fact the potential difference across the Korea Strait as the cable was grounded at Hamada and Busan using copper electrodes (Fig. 2). Cable voltage measured every 5 min. at Busan is available on a real-time basis through the internet homepage (http://eastsea.snu.ac.kr) of the Ocean Circulation Research Laboratory, Seoul National University (SNU).

The observed voltage and whole-strait currents have prominent peaks in their power spectra at diurnal and semidiurnal tidal frequencies (Fig. 3). At low frequencies, spectral energy density is high, especially at subinertial and monthly timescales involving voltage levels. One can notice in the voltage spectra, however, that there are significant peaks at frequencies of 3, 4, and 5 cycles per day (cpd), which are not significant in the spectra of the whole-strait currents. These variations may be related to the solar diurnal variations in geomagnetic fields at 1, 2, 3, 4, and 5 cpd as reported by Larsen (1992). Since these geomagnetic effects on the observed voltage are significant at timescales shorter than 5 days according to Larsen (1992), they must be removed from the observed voltage to investigate oceanographic tidal and subinertial variations (Kim *et al.* 2004b). The geomagnetic-induced voltage, which is considerable over periods shorter than two

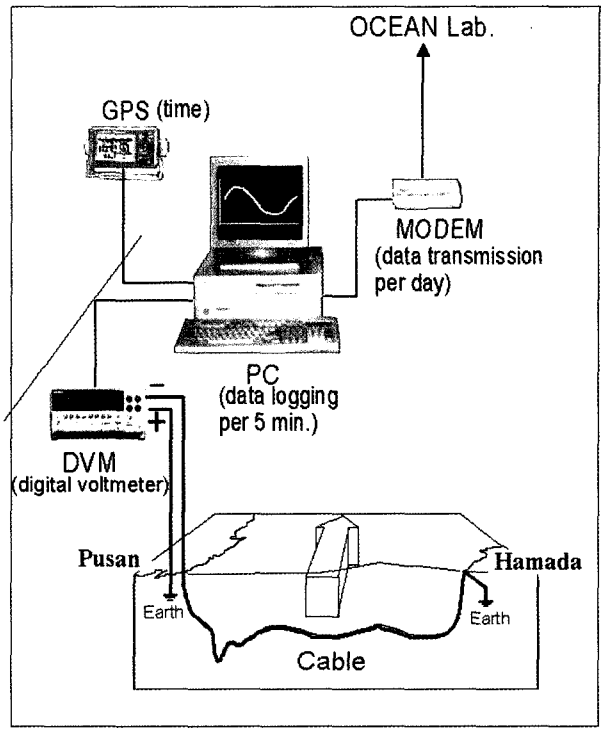

Fig. 2. Cable voltage measurement system at the Busan Submarine Cable Relay Station.

days, could be removed from those readings measured by the methods of Larsen *et al.* (1996.). More details on the geomagnetic correction were given by Kim *et al.* (2004b).

Transport variability across the Korea Strait

The residual voltage is compared with observed transports based on moored ADCP measurements (Jacobs *et al.* 2001) and the vessel-mounted ADCP (Takikawa *et al.* 1999) after low-pass filtering with a half-power of 36 h and sub-sampling every 3 h. Fig. 4 shows that there is a very good linear relationship between voltage and the observed transports from both the bottom-moored ADCPs and the vessel-mounted ADCP. The conversion factor from voltage to transport is estimated to be V=(8.06±0.63) Sv V^{-1} ($1Sv=1\times10^6 m^3 s^{-1}$) with the bias voltage of V=0.48 ±0.07 Sv V^{-1} (Kim *et al.* 2004b). There are transport variations as large as 2~3 Sv on timescales of 3~7 days. It should be pointed out that these subinertial variations are larger than the known seasonal variations in the Korea Strait (Takikawa *et al.* 1999; Teague *et al.* 2002). Lyu *et al.* (2002a) reported that these variations are related to nonisostatic responses of the East Sea to the atmospheric pressure forcing.

To investigate seasonal variations, a low-pass filter with a half-power period of 90 days is applied to the voltage-

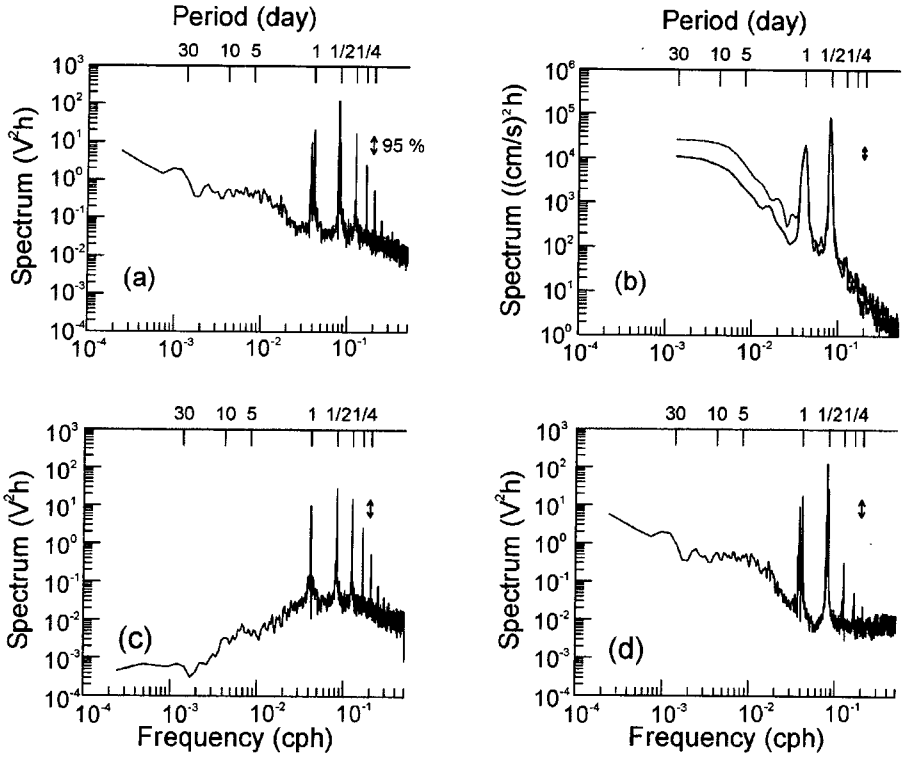

Fig. 3. Power spectrum with 95% confidence interval of (a) raw voltage, (b) depth-averaged, along-strait current measured at the N2 station (see Fig. 1, Teague *et al.* 2002 for location) for the first (dark line) and second (light line) half of the ADCP records by the US NRL, (c) geomagnetic-induced voltage, and (d) corrected voltage.

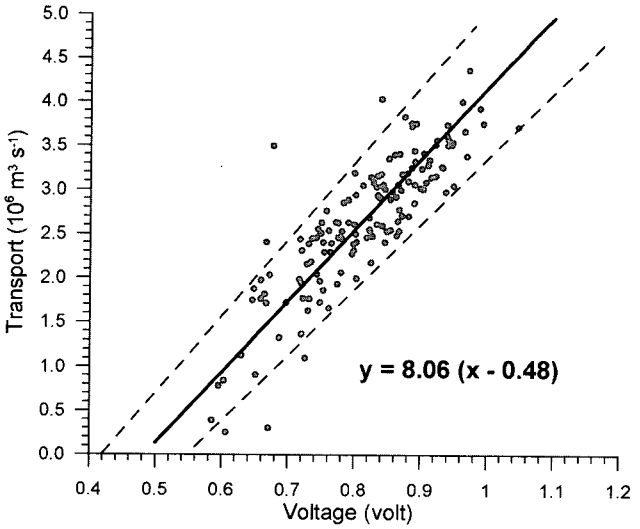

Fig. 4. Linear regression between transport observed by the bottom-mounted ADCPs (Teague *et al.* 2002) and voltage data measured on submarine cables through the Korea Strait. 144 data in each data set is used after low-pass filtering with a half-power period of 36 hours and subsampling every 2 days. The thick solid line is the linear regression line and dashed lines represent standard error bounds. (from Kim *et al.* 2004b).

derived transport induced by the conversion factor and the bias voltage. There are also large variations in the transport with a range of 2 Sv over timescales measuring about a month. Seven-year data show a relatively larger transport in summer and autumn than in winter and spring, but there is a large interannual variation (Fig. 5). The seasonal variation is very weak from spring 2000 to fall 2001, and annual mean transport is reduced by 0.4 Sv from 1999 to 2000.

The disappearance of the northward flowing East Korean Warm Current (EKWC), which has been thought of as a permanent branch of the Tsushima Current flowing northwards along the east coast of Korea, occurred between mid-June and early November 2000 based on PIES (Pressure-equipped Inverted Echo Sounder) data, so the EKWC was absent for five months (Chang *et al.* 2004). It is noted that the transport through the Korea Strait was small during this period compared to the same period of 1998-1999. The cable voltage data provides a good means of monitoring the transport through the Korea Strait continuously and enables us to investigate various temporal transport variations and their causes, which exert a major influence on the circulation and the hydrography of the East Sea (Kim *et al.* 2004b).

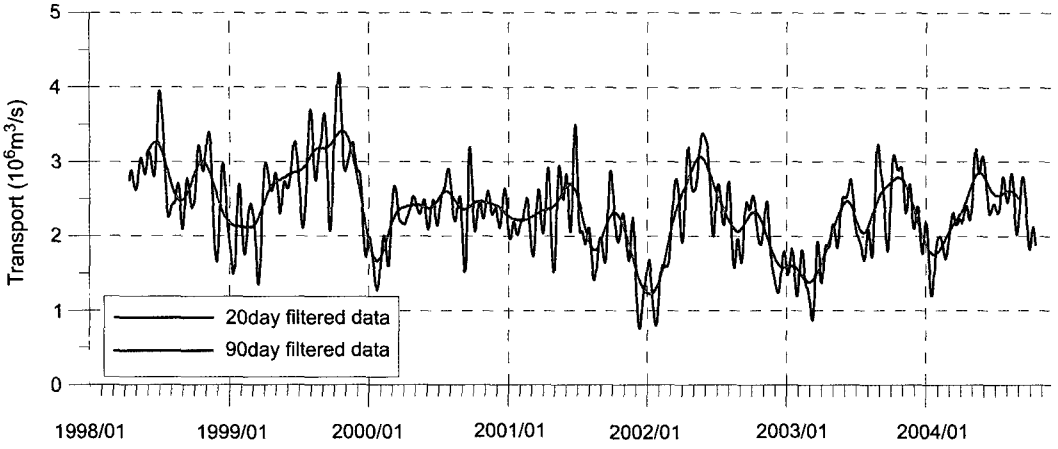

Fig. 5. Seasonal variations of voltage-derived transport after low-pass filtering with a half-power period of 20 days and 90 days.

3. ARGO Profiling Float

The ARGO profiling float is a neutrally buoyant float that measures subsurface ocean currents and profiles temperature (T) and salinity (S) in the vertical. Since 1997, about 90 autonomous floats have been deployed in the JB and UB of the East Sea by Seoul National University, the University of Washington, KORDI, and the Korea Meteorological Agency (Fig. 6). Those floats have provided profiling observations of T and S every 7~10 days while drifting with deep currents mostly at depths of 700~800 m. To utilize both trajectory and profile data from ARGO floats, we have developed new data processing techniques such as how to control the quality of T/S profile and trajectory, how to estimate deep currents accurately, and how to obtain surface currents from trajectory data. In this section, the techniques for extracting valuable information from ARGO floats and some preliminary results are briefly presented.

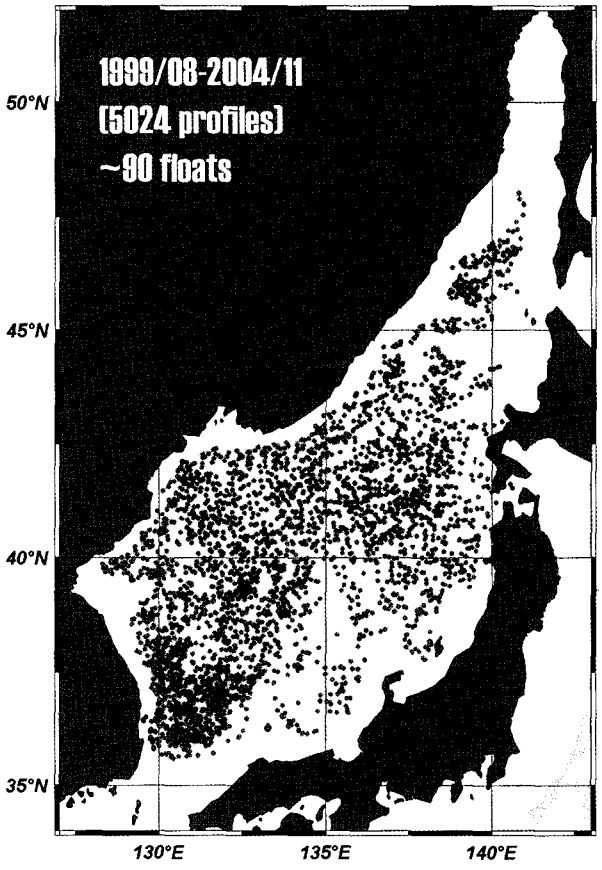

Fig. 6. Station map of profile data from ARGO floats in the East Sea from 1999 to 2004.

Salinity quality assessment and control in the East Sea

In the international ARGO program, numerous profiling floats have been deployed in the world ocean since 2000, which are aimed at obtaining spatial and temporal resolution of 300 km over 1 month in the near future. However, in the East Sea, we have assembled more than 5000 profiles from 1999 to 2004 which have the resolution of 100 km for a period of 1 month on average (Fig. 6). Furthermore, since the high resolution Conductivity-Temperature-Depth (CTD) measurement in CREAMS experiment has been conducted almost every year from 1992 to 2004, the East Sea has become a good basin for evaluating the quality of the salinity profile data from ARGO floats.

The ARGO floats are expected to give good measurements of temperature and pressure, but salinity measurements may suffer sensor drifts owing to biofouling and various other problems. Wong *et al.* (2003) and Kobayashi *et al.* (2001) reported a method for calibrating salinity data for ARGO floats drifting in the Atlantic and Pacific Oceans, respectively. Although the T-S relationship in the East Sea

is similar to that of the open oceans, vertical and horizontal variation of salinity for deep waters is of the order of 0.001, one order of magnitude smaller than that of the open ocean (Kim *et al.* 2004a). Moreover, water mass in the upper 1000m has experienced a rapid change in property over the last 50 years, so the T-S relation at present has even further difference from those of the 1960s. Thus, accurate and high-resolution CTD profile data, which were recently measured, are required to assess salinity measured by ARGO floats in the East Sea.

High quality data taken for more than 10 years through CREAMS expeditions can provide mean and natural variability of salinity over the whole East Sea, so we utilized the CREAMS CTD data for the assessment and calibration of salinity measured by ARGO floats. Because most ARGO floats have been deployed since 1999 in the East Sea, the CTD data from CREAMS in 1992~1999 (Feb.) are used to calculate ground salinity values at the parking depth and those in 1999 (Sep.) ~2004 to evaluate the accuracy of the corrected salinity from floats (Fig. 6).

The most important part of salinity quality control procedure is to correct the bias in the salinity profile. Fig. 7 presents the salinity deviation below 400m from high-resolution CTD data with a ±10-day window and 20 km radius. Non-corrected salinity data clearly has a freshening bias relative to CTD data and a non-Gaussian distribution with a standard deviation of 0.07. On the contrary, the correction yields the improved salinity data with one standard deviation error of 0.006, which clearly has a normal distribution of population (Park *et al.* 2002).

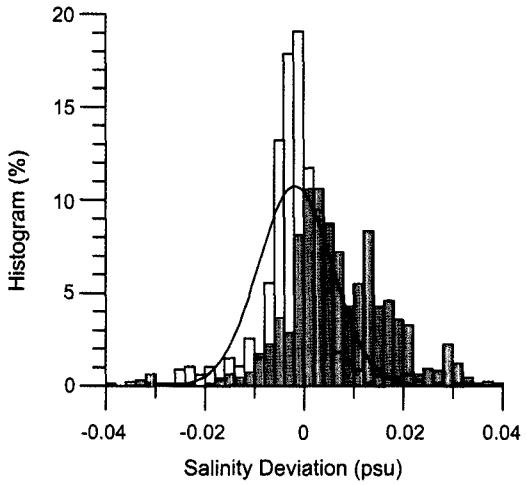

Fig. 7. Probability distribution of salinity difference from between ARGO floats (blue open boxes: corrected, red boxes: non-corrected) and high resolution CTD data in the layers deeper than 400 m. Solid curve presents a Gaussian function fitted to the histogram of corrected float data.

Deep current estimation using trajectory data

The ARGO profiling floats drift with the deep current for about 7~10 days and convey oceanic and engineering data to satellites while drifting on the surface. It then descends to the parking depth and drifts again. After a float reaches the sea surface, it drifts an unknown distance at the surface before its position is determined by an ARGOS satellite. Similarly, floats drift away after their last contact with a satellite before they start to dive. In principle, deep currents are estimated by dividing the distance floats moving at parking depths by the duration of drift, which requires knowledge of the time and positions of diving and surfacing (not directly measured). Since currents are much stronger at and near the surface than at parking depths, the unknown drift before the first fix and after the last fix, while floats are at the surface, provide a significant source of error in estimating the deep currents.

The time of diving is obtained from the reference time (dive time at the first cycle). If this is not available as part of the float metadata, a method is given for determining it from the collection of times given for float position fixes. The time of surfacing can be estimated from the float park duration and ascent rate, or preferably calculated from data in the float engineering data message (Park *et al.* 2005).

Surface and dive positions are estimated by extrapolating observed positions to the surfacing and diving times. A method is presented in which the surface trajectory is assumed to be a combination of linear and inertial velocity. The velocities are calculated explicitly for each surface trajectory from the float data. A full surface trajectory reproduced by the summation of the velocities would provide the positions with an uncertainty level of 1.7 km at which a float might surface and dive.

The calculation of mean subsurface velocity from surface positions assumes the entire subsurface period is spent at the park depth. We have examined geostrophic shear between the park depth and the surface, and estimated the additional displacement during the ascent and descent. In the East Sea, this was found to be of the order of 100 m, which can be ignored. We note that an error of about 1 km in determination of the displacement over a 10 day period is equivalent to approximately 0.1 cm s^{-1}. Therefore, we suggest that all errors combined should result in individual subsurface velocity estimates with an uncertainty of the order of 0.2 cm s^{-1}. More than 90 floats that have been deployed in the East Sea can provide accurate deep current data with an unprecedent amount of high spatial coverage.

Inertial kinetic energy from ARGO float data

As a by-product of deep current estimation, we obtain an inertial current from ARGO float trajectory at the sea

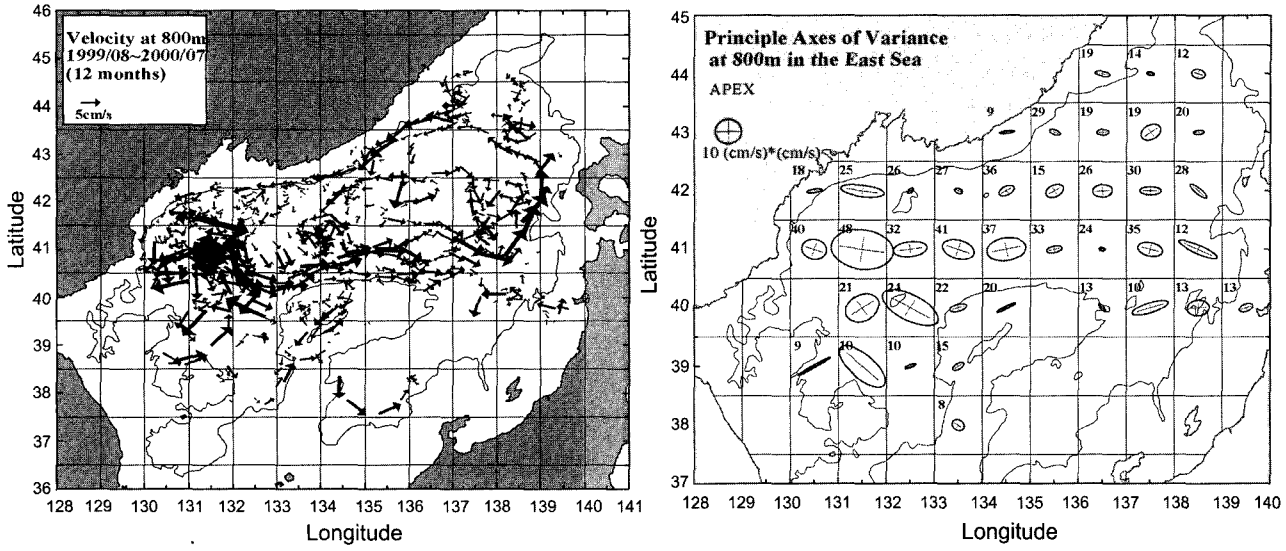

Fig. 8. Example of deep currents obtained from profiling floats in the East Sea in Aug. 1999~Jul. 2000 (Left panel). Map of eddy kinetic energy and principle axis in the Japan basin (Right panel) in 1999~2003.

surface. Through the comparison of inertial amplitudes from satellite-tracked surface drifters and error estimation from numerical simulation, the inertial amplitude could be estimated within an uncertainty variable of about 3.4 cm s^{-1} (Park *et al.* 2004). Furthermore, since ARGO floats observe both surface trajectory and T/S profile at the same time (to within a few hours), the inertial amplitude and the mixed layer depth (MLD) estimated from the surface trajectory and T/S profile of an ARGO float enable us to calculate the inertial kinetic energy in the mixed layer under the assumption that the inertial current is homogeneous in the mixed layer. A time-series of ARGO array data may give us the means to understand large-scale distribution of inertial motion and energy in the East Sea as well as in the global ocean. The probability of inertial amplitude is found to be highly non-Gaussian and intermittent. The magnitude of inertial currents in the East Sea reaches 14.3 cm s^{-1} on average and ranges from zero to a maximum value of 80 cm s^{-1}. Mean inertial kinetic energy estimated from the floats in the East Sea is about 1288 J m^{-2} which has a similar size to that of the mid-latitude of the North Pacific (1294 J m^{-2}) and is slightly larger than that of the global mean energy (1164 J m^{-2}). Park *et al.* (2005, in preparation) reports a large-scale distribution of inertial amplitude in space and time mostly dependent on the MLD conditions despite the generation of inertial currents due to local wind stress. However, the meridional difference of zonal averaged MLD in the North Pacific is too small to contribute to the spatial distribution of inertial amplitudes.

Subsurface currents and water masses

ARGO float data provide deep circulation patterns in the East Sea, which cannot be achieved from spatially-limited current meter moorings. The subsurface circulation at 800 m in the Eastern Japan Basin is primarily cyclonic along the bathymetry in all seasons, which is similar to the surface circulation derived from trajectories of satellite-tracked surface drifters. Currents in the Western Japan Basin provide little indication of significant mean field from the floats. They are more variable in direction and their magnitudes are larger than those in the Eastern Japan Basin (Fig. 8). Seasonal variation of circulation at 800 m in the Eastern Japan Basin is not so obvious, while velocities in the Western Japan Basin seem to have some seasonality (Park *et al.* 2002).

Quality controlled salinity data from the profiling floats provide enough accuracy to examine the variations in the intermediate waters, which have been found in the East Sea by Kim *et al.* (1999). Particularly, using CREAMS hydrographic data (winter 1999) and profiling float data (1999~2003) obtained in the Japan Basin, the change in High Salinity Intermediate Water (HSIW) properties over about 5 years are investigated (Fig. 9). The HSIW thickness map from 1999 to 2003 shows that the HSIW is mostly distributed within the Eastern Japan Basin (135~139°E, 41~44°N). The HSIW with high temperature (2~2.5°C) and salinity (~34.1) appeared in 2001 and 2002. The high salinity water advected from the south at the surface layer in the preconditioning phase determined the surface water property in the late winter, 2000 and 2001. These are associated with warm-saline HSIW in the

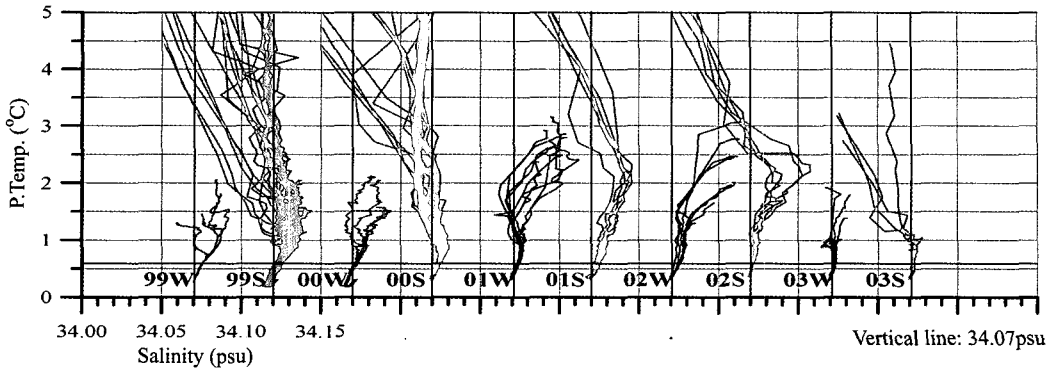

Fig. 9. T-S diagrams within a bin of 136.5~138.5°E, 41.5~43°N from 1999 to 2003. This shows inter-annual variability of HSIW defined as 0.6~5°C, more than 34.07. Light blue (from CTD) and dark blue (from floats) lines are in winter. Red (from CTD) and orange (from floats) lines are in summer. Vertical sold lines in black stand for 34.07.

following summer, 2001 and 2002, respectively. However, even though cold (~1°C) and less saline (~34.08) HSIW was observed in the winter and summer of 1990 and 2000, we could not find any Tsushima Warm Water (5~15°C, >34.08) over this region in late autumn, so the HSIW in 1990 and 2000 might be formed mostly by air-sea interaction (Park *et al.* 2003).

4. East Sea Real-time Ocean Monitoring Buoy

Development and operation

In order to monitor ocean variability in real-time and to elucidate relevant processes, the East Sea Real-time Ocean Buoy (ESROB) has been developed and successfully operated near the Donghae city, Korea (Fig. 10), at a depth of about 100 m (10 km off the coast) since 1999

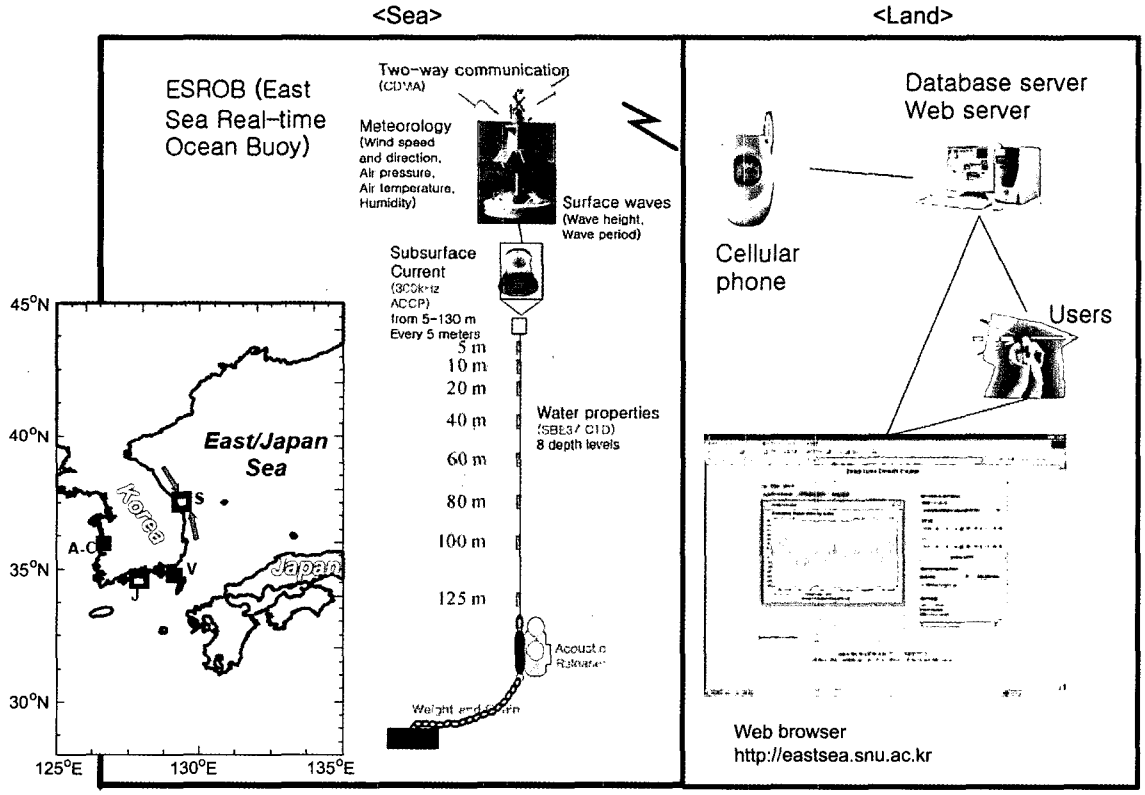

Fig. 10. Location ('S' in the left map), mooring design, measuring variables, and data flow of the ESROB.

(Kim *et al.* 1999). It is of great importance scientifically to acquiring long and continuous time series data, especially in this region because the area is known for high spatial and temporal variability due to the convergence of the North Korean Cold Current (NKCC) and the East Korean Warm Current (EKWC) as well as various coastal ocean processes. Owing to successful operation of the ESROB in the region, similar coastal ocean monitoring buoys are under development in key areas around the Korean Peninsula.

The size of ESROB is 2.5 m in diameter (1.8 m for ESROB1a in 1999). The design of ESROB is shown in Fig. 10, consisting of surface 'air' part with meteorological sensors (four solar panels for power supply, navigation light and radar reflector, and antennas for DGPS and telemetry) and subsurface 'ocean' part (inductive lines for CTD data transfer, chain and anchor for stable mooring, and acoustic releaser for safe recovery with various oceanographic sensors).

Meteorological sensors measure wind speed, gust (maximum wind speed for 10 min.) and direction, air temperature and pressure, and relative humidity every 10 minutes. Surface waves are parameterized every 10 minutes from 1,024 accelerometer data measured in 2 Hz. Three-dimensional subsurface currents at 26 vertical levels are measured every 1 to 10 minutes using 300 kHz ADCP looking downward below the bottom of the buoy frame. Several SBE37 CTDs are attached to the inductive mooring line, acquiring profile data for physical properties (T and S) of seawater every 1 to 10 minutes. Besides meteorological and oceanographic data, it measures real-time operational status for maintenance; buoy power (battery) levels, communication antenna levels, internal temperature and humidity, buoy position, attitude (heading, pitch, and roll), speed and direction (calculated from the position changes occurring over 10 minutes).

All the data measured at each sensor are transferred to the main controller every minute, and are transmitted in real-time to the database server in the laboratory using Code Division Multiple Access (CDMA) cellular phone communication (Fig. 10). The CDMA communication enables us to control ESROB monitoring through two-way transmission. For example, if a user wants to sample data for a 1 min. interval for a specific period, one can change the sampling time interval from 10 min. (default sampling interval) to 1 min. for the period by sending specified short message commands to the ESROB. In addition to a sampling interval change, alarm position (when the ESROB moves outside the specific area), switching on and off sensors, checking status, etc. are all available by sending short commands to the ESROB using two-way CDMA communication. The ESROB data stored in the database server are again transferred to the web server and provided to the public in real-time (Fig. 10) through the websites (http://www.otronix.com, *or* http://eastsea.snu.ac.kr).

Technical advances enabled safer and more effective monitoring of ESROB than before. Major technical achievements since 1999 are two-way communication using a CDMA cellular phone for data transmission, measurement of currents for the entire water column using a downward-oriented ADCP, integration of wave sensor and CTD sensors at 8 depth levels (5, 10, 20, 40, 60, 80, 100, and 125 m) for monitoring surface waves and profiling of water properties, and user objective real-time provision of the data through the websites. Major technical progress in the ESROB operations are summarized in Table 1.

Results from ESROB data

The ESROB data exhibit multi-scale oceanographic variability, which are related to (known and unknown) ocean processes. Preliminary analysis provides evidence for 1) southward or southeastward NKCC in the region; 2) on- and off-shore movement of EKWC relevant to its meandering; 3) transient, wind-driven barotropic jet; 4) coastal upwelling and downwelling related to baroclinic

Table 1. History of ESROB (East Sea Real-time Ocean Buoy) operations

Year	Buoy ID	Period of operation	Major technical progress
1999	ESROB1a	Apr.25-Jun.27, Aug.26-Sep.23	Current measurement at 4 depths
2000	ESROB1b,c	Apr.7-May 30, Jun.14-Sep.13	Current measurement at 20 depths
			CTD attachment at 4 depths
2001	ESROB2	Apr.7-Sep.25	CTD attachment at 5 depths
2002	ESROB3	May 4-Aug.29	Change in telemetry (UHF→CDMA)
			Attachment of wave sensors
2003	ESROB4	Jan.13-Oct.5, 2003	Two-way control using cellular phone
			Current measurement at 26 depths
	ESROB5	Oct.13-Dec.17, 2003	Attachment of biogechemical sensors
		Apr.1-Sep 3, 2004	CTD attachment at 8 depths
		Dec.15, 2004.-Present	Stable operation

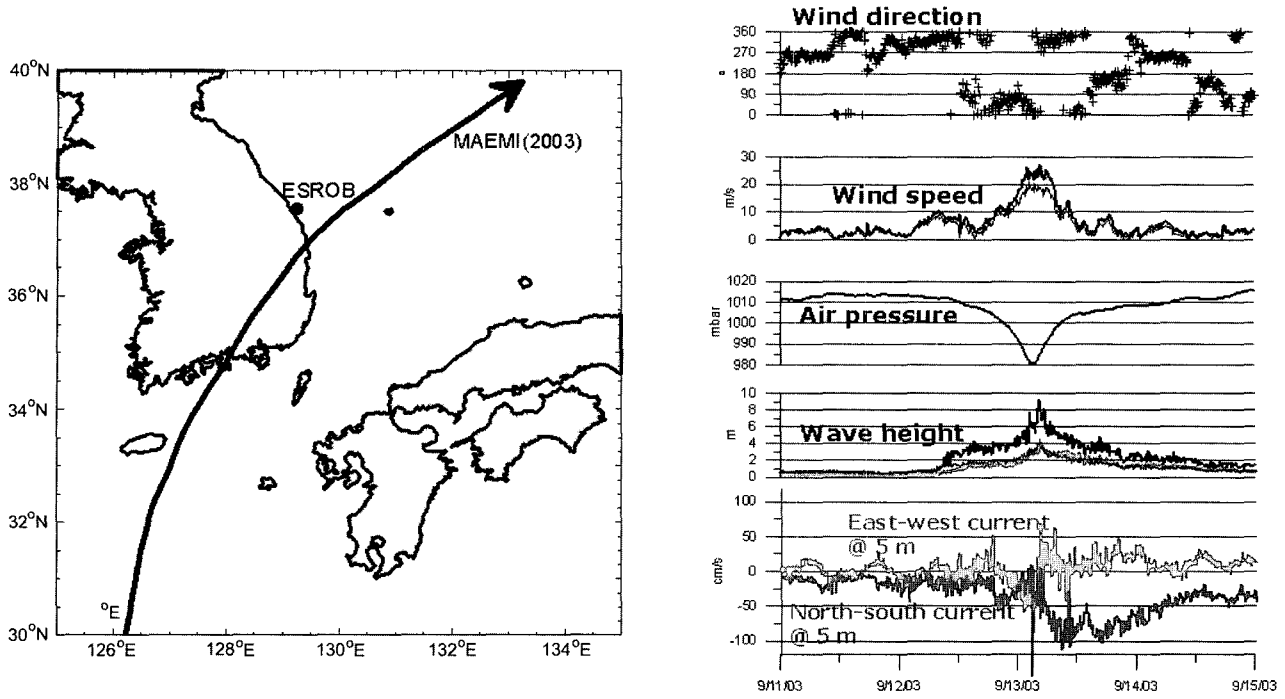

Fig. 11. (a) Path of the eye of typhoon 'MAEMI' and (b) time series of wind direction (in degrees clockwise from the north) and speed, air pressure, wave height, and east-west and north-south current measured from the ESROB during the passage of 'MAEMI' in September, 2003.

jet; 5) propagation and reflection of near-inertial internal waves and semi-diurnal internal tides; 6) generation and propagation of internal solitary waves near buoyancy frequency, and 7) temporal variability of sea surface wind and surface waves in the region.

The influence of major current systems — EKWC and NKCC — is well represented from the monthly-averaged ADCP data. Southward or southeastward currents prevailed at all depth levels (especially at lower depth levels) during the entire observational period from 1999 to 2004. Water properties observed for the period of southward or southeastward currents are mostly similar to those of the North Korean Cold Water (NKCW) based on the Kim and Kim (1983)'s definition (temperature of 1-6 °C and salinity below 34.00). The southeastward currents often occurred below 50 m (in a water depth of 100 or 130 m) with a speed of about a few cm s^{-1} so that the current could be regarded as the upper part of NKCC, considering its position and strength (Kim and Kim 1983). In contrast to the predominace of NKCC in the coastal region for most of the observational period, the northward or northwestward monthly-averaged current occurred sometimes near the surface, as in March, April and July in 2001, and February to May, and August to December periods in 2003. SST images indicated the EKWC approached the coast in those months. Though the speed of northward or northwestward mean currents observed from the ESROB is much smaller (one or two order less) than typical EKWC speeds of about 1 m s^{-1} at the core, the northward or northwestward mean currents near the surface seem to occur due to the onshore penetration of the EKWC.

At a period of a few days or a week, depth-averaged current variations observed from the ESROB are mostly polarized in the alongshore direction, and the alongshore current fluctuations are correlated to wind fluctuations, indicating the wind-driven barotropic responses in the region. The regression analysis revealed that the speed of the barotropic wind-driven coastal jet reaches 10-30 cm s^{-1} corresponding to about 3% of alongshore wind speed for moderate wind conditions (wind speed of 3-10 m s^{-1}) as the theory on frictional response of the coastal ocean to the alongshore wind suggests (Csanady 1984). Depth-dependent current variations at the period of a few days or a week are mostly related to the coastal upwelling and downwelling response to cumulative wind stress at the surface. For a coastal upwelling (downwelling) favorable wind, which is offshore (onshore) or northwestward (southeastward) wind stress in the region, the ESROB recorded offshore (onshore) currents in the upper levels and onshore (offshore) currents in the lower levels. In the alongshore direction, a strong baroclinic jet occurred in the upper levels much strengthened in the same direction of wind

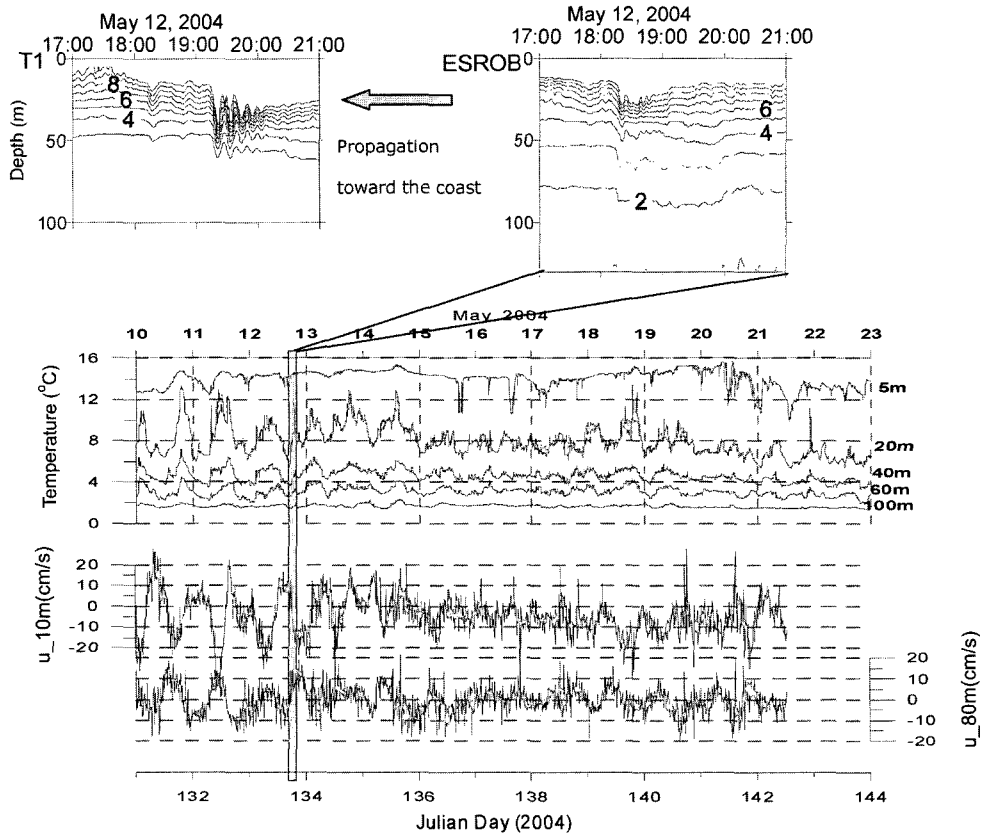

Fig. 12. Time-depth contour of water temperature measured near Donghae City, Korea, at a water depth of 100 m (T1) and 130 m (ESROB) for 17:00-21:00 12 May 2004. Time series of temperature measured at 5 depths (5, 20, 40, 60, and 100 m) for ESROB and cross-shore currents at 2 depths (10 and 80 m) for 10-23 May 2004.

stress, accompanied by enhanced vertical shear. Moreover, the CTD data observed from the ESROB and also other field experiments in the region, showed that the isotherms, isohaline, and thus isopycnals sloped up (down) toward the coast during the upwelling (downwelling) events. Typical magnitudes of cross-shore density gradient (~0.1 kg m^{-3} over the distance of 5 km) and temporal change of density (~0.1 kg m^{-3} over the time scale of 5 day) are all consistent with the vertical shear of alongshore currents and cross-shore currents (~O(0.001 s^{-1})) based on the linear theories (Csanady 1984), *i.e.* thermal wind balance, etc.

These wind-driven responses in this region are well captured when the typhoon 'Maemi' passed by near the ESROB site on 13th September 2003 (Fig. 11). The ESROB recorded a maximum wind gust of 25 m s^{-1} (10 minutes' average speed of 20 m/s) and a minimum air pressure of 980 hPa when the eye of 'Maemi' was located at Uljin, Korea at 03:00 (Fig. 11). Along with the wind directions of 0-90° (northeasterly) and 270-360° (northwesterly) before and after the eye passage respectively, the meteorological parameters indicate that a strong northerly wind blew at that period. The currents measured near the surface reached up to about 100 cm s^{-1} in the southward direction at 13:00 (10 hours after the passage of 'Maemi') (Fig. 11). Accompanied by strong southward currents, thickness of the mixed layer (characterized by high temperature and low salinity) gradually increased from 20 m to 40 m over the 10-hour period. A simple two-layer model for the response to an impulsive alongshore wind over an uniformly sloping bottom developed by Csanady (1984) showed reasonable estimates of alongshore and offshore currents and interface displacement under the condition of the 'Maemi' passage at the location over a 10-hour period (Nam *et al.* 2004b). This model result also confirmed a downwelling type response to southeastward wind stress (downwelling favorable wind condition) in the region, reproducing such a strong baroclinic jet at the upper layer in the alongshore direction.

One of the most striking features observed from the ESROB data is an intermittent internal wave motion at the near-inertial, semi-diurnal, and near-buoyancy periods, which are 17-19 hours (where the local inertial period is 19.6 hours), about 12 hours, and several to tens of minutes, respectively. The intermittent modulations of current fluctuations in magnitude of O (10 cm s^{-1}) were often

observed in the ADCP data at the near-inertial and semi-diurnal periods (Fig. 12), even though the barotropic (both diurnal and semidiurnal) tidal current in the region is very weak (~5 cm s^{-1}) based on the harmonics of both tide gauge sea levels and depth-averaged currents. Near-inertial and semi-diurnal wave motions are also recognizable from the CTD data, which show the intermittent vertical displacement of isotherms of O (10 m) at those periods (Fig. 12). In addition to near-inertial and semi-diurnal internal waves, the ESROB also evidences the generation and propagation of internal solitary waves with periods of a few or few tens of minutes (Fig. 12). Abrupt temperature changes (within an hour) with enhanced vertical shear of horizontal currents are caused by the passage of the internal solitary waves in the region. The temporal variations of isotherms are similar to those due to the internal solitons observed by Kim *et al.* (2001) in this region. Fig. 12 shows enhanced cross-shore currents at a near-inertial period from May 10 to May 15, 2004, which is nearly out of phase between the two depths, and the packet of internal solitary waves is generated as they propagate towards the coast (water depth from 130 m to 100 m) on May 12, 2004.

Besides the CTD and ADCP data obtained from the ESROB, wind and surface wave data could be investigated together with the satellite measurement such as scatterometers (Park *et al.* 2003) and synthetic aperture radar (Kim *et al.* 2003) for better understanding of spatio-temporal variability of sea surface wind and waves near and off the coast (Kim *et al.* 2004c; Nam *et al.* 2004c). Continuous ESROB monitoring will certainly contribute to the progress in our knowledge of coastal ocean variability in the East Sea.

5. Moored Current Measurements in the Southwestern East Sea

The UB is surrounded by shallow topographic features; the Korea Strait shallower than 200 m to the south, Oki Bank shallower than 100 m to the east, and the Korea Plateau shallower than 1500 m to the west (Fig. 13, redraw). The maximum depth of the UB exceeds 2200 m, and the 2000 m isobath from the JB continues into the UB through a narrow constriction between Ulleungdo and Dokdo called the Ulleung Interplain Gap (UIG), a deep (ca. 2,500 m deep and 90 km wide) passage between the UB and JB. A map of bottom potential temperature (Chang *et al.* 2002a) indicates that the dense deep flow into the UB, colder than 0.1 ℃ (the East Sea Deep and Bottom Waters according to Kim *et al.* 1996), must take place through the UIG. Attempts have been made to monitor the deep flow through the UIG through the deployment of current meter mooring lines since 1996 (Chang *et al.* 2002b), and the current moorings are still

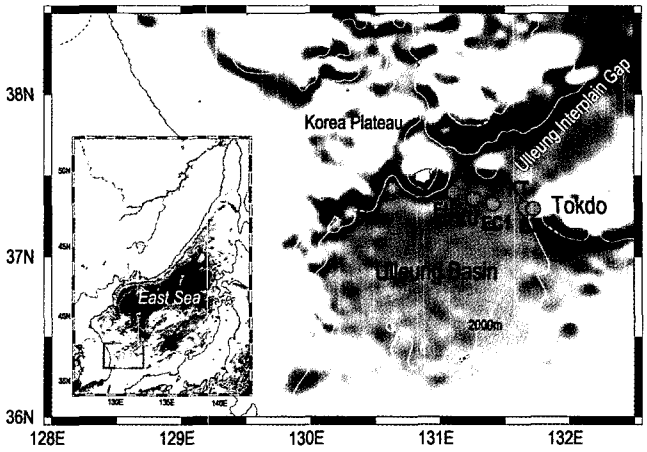

Fig. 13. Bathymetry of the Ulleung Basin, and current meter mooring locations in the Ulleung Interplane Gap during November 2002 and April 2004. Mooring at EC1 has been in operation since November 1996. Currently moorings at EC1 and ET are in operation.

in operation. According to continuous bottom pressure and current measurements in the UB between June 1999 and June 2001, deep currents are characterized by a short correlation scale and the predominance of mesoscale variability over periods of 20~40 days (Chang *et al.* 2004). The deepwater flux and its variability in the UIG are thought to be an important constraint on the general circulation of the UB, the observed variability of deep circulation, and vertical mixing of the deepwater currents. In the following, we introduce the mooring works to monitor the deepwater flux through the UIG and some results on the spatio-temporal structure of deepwater circulation and currents in the UB including the UIG.

Monitoring program in the Ulleung Interplane Gap

Deep currents have been measured in the central UIG (station EC1) since November 1996, except for a missing period between May and November 2002, using a taut-wire subsurface mooring line typically equipped with three current meters at around 400 m, 1400 m, and 20 m above the seabed (Fig. 14). An upward-looking ADCP was set up at the top of the mooring line to measure currents simultaneously in the upper 200 m for mooring periods during October 2001~May 2002 (Leg 8) and November 2002~April 2004 (Leg 9). Subsurface currents at EC1 show a predominance of southwestward flow below 400 m depth with occasional reversals on short timescales. Chang *et al.* (2002b) conjectured a net inflow of about 0.5 Sv into the UB through the UIG below 1500 m using measured current data at EC1, which yielded a large upwelling rate and a diapycnal mixing coefficient. A high-resolution numerical model, however, predicts the

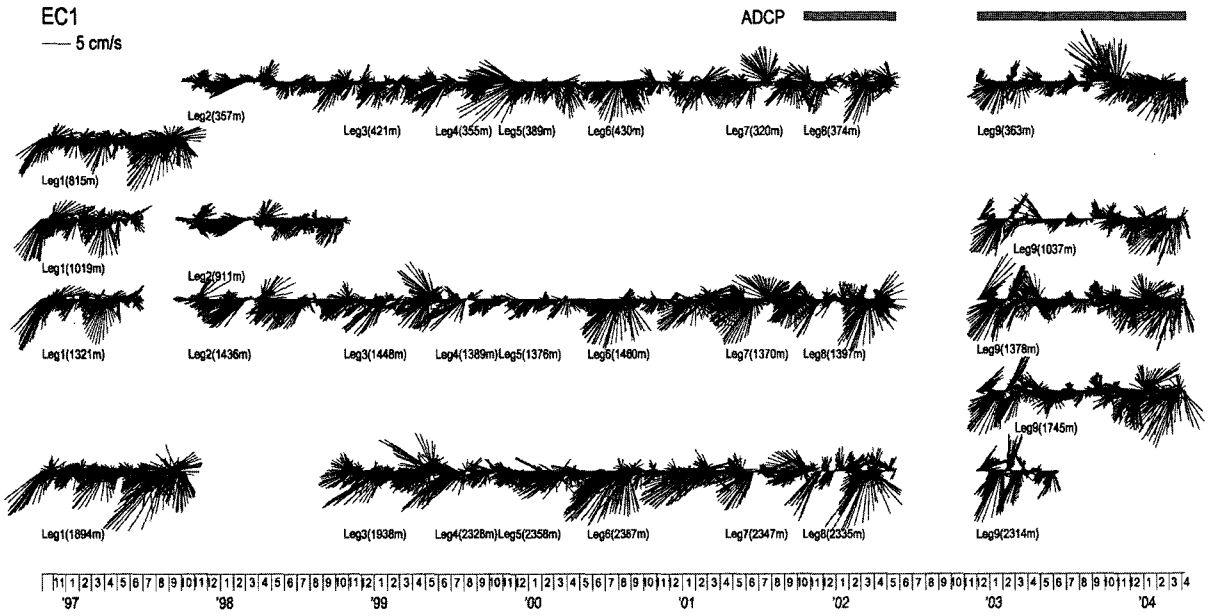

Fig. 14. Vector time series of low-pass filtered deep currents at EC1. North is positive on the y-axis, and current meter mooring depths are shown in parentheses. Periods of upper current measurements using acoustic Doppler current profiler (ADCP) are denoted by grey bars.

deep flows into the UB in the western UIG near Ulleungdo and those out of the UB in the eastern UIG near Dokdo (Hogan and Hurlburt 2000), suggestive of the necessity for measuring flows over the entire UIG to quantify the deepwater flux. Along with the mooring at EC1, two additional mooring lines both equipped with one current meter near the seabed were deployed near Ulleungdo (station EU) and Dokdo (station ET) in April 2001 (Legs 7, 8). Two moorings at EC1 and EU were recovered in May 2002, but the mooring at ET was lost. Bottom currents at EU are not stably as southwestward in their orientation as those at EC1, instead, southward and northward flows alternate, with record-length (~13 months) mean currents being directed to the west. An array of five current meter moorings, each of which was equipped with two current meters at around 1800 m and 20 m above the seabed, were deployed in November 2002 for reliable flux estimates of the deep water through the UIG (Leg 9). The five moorings were successfully recovered in April 2004. Data from these moorings, which will be described shortly, show strong northward flows close to Dokdo. Preliminary analysis of the data indicates that moorings at EC1 and ET could represent the southward and northward transports, respectively, and those two moorings are currently in operation to monitor the deepwater flux through the UIG.

Deep circulation and currents in the Ulleung Basin

Bottom pressure and velocity measurements for two years show that the deep circulation in the UB during the seasonal to annual time scales is mainly cyclonic with additional cyclonic and anticyclonic cells on sub-basin scales (Chang *et al.* 2004; Teague *et al.* 2005). A strong and stationary cyclonic cell occurs along the continental slope off Korea. Strong bottom currents, that sometimes exceed 10 cm s^{-1} with a maximum of 18.5 cm s^{-1}, are observed on the western side of this cyclonic cell. There is a weaker but stationary anticyclonic cell around Ulleungdo. A strong northward flow over the Korea Plateau between Ulleungdo and the east coast of Korea is associated with this anticyclonic cell. Strengthening and weakening of these two counter-rotating cells and their mutual interaction and interaction with the upper circulation have not yet been clarified. Horizontal coherence in the measured deep flows is small. Seasonality is indistinct, while mesoscale variability with periods of 20-50 days is dominant in the observed current fluctuations.

Fig. 15 shows subtidal current vectors measured at five moorings across the UIG during Leg 9. Velocity was not obtained at a depth of 1800 m on mooring ET due to the trouble associated with the data storage unit. Data were not recorded for the entire measurement period near the seabed at moorings EC1 and KT due to battery problems. Deep currents are mainly directed to the south or southwest at three moorings EU, KU, and EC1 on the west with the strongest flow at EC1, and to the north at two moorings KT and ET on the east with the strongest flow against the eastern wall near Dokdo. The northward

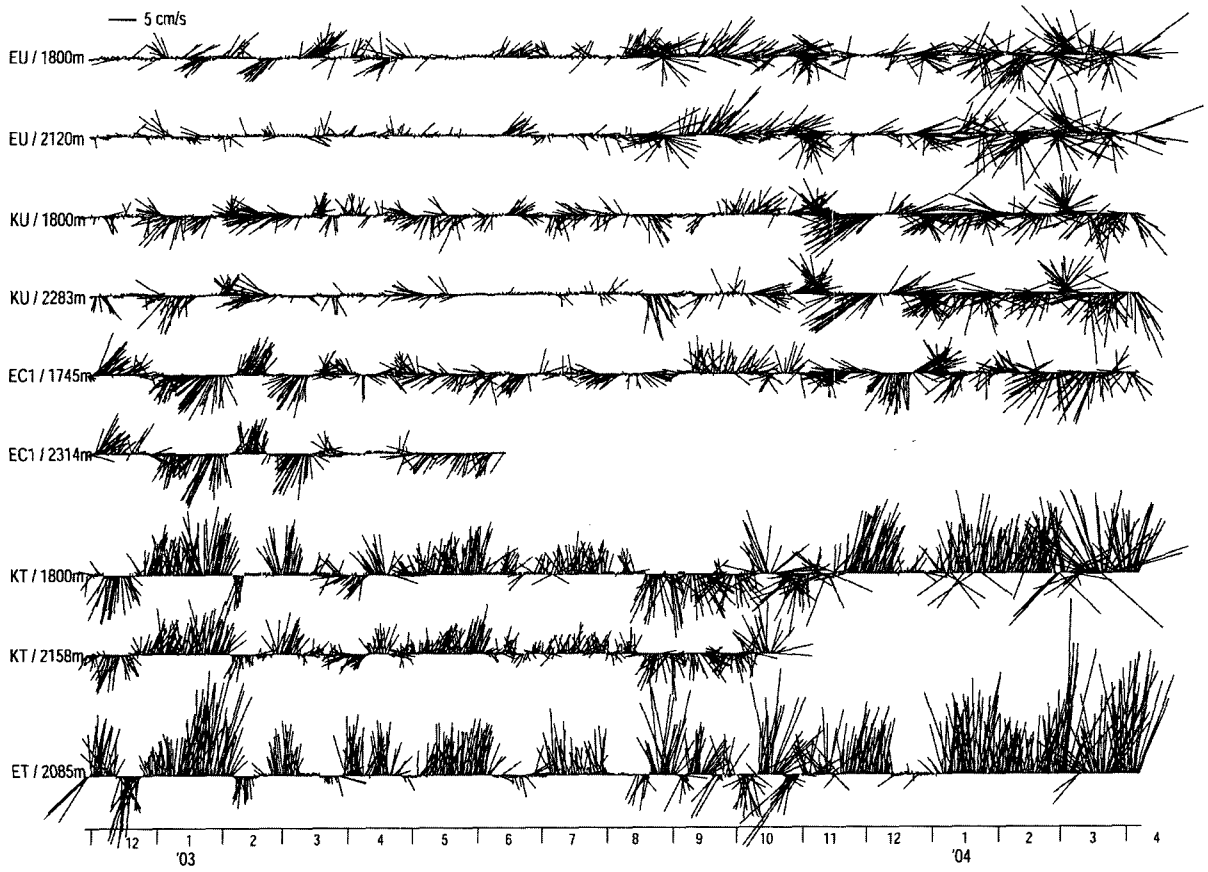

Fig. 15. Vector time series of low-pass filtered deep currents measured at five moorings in the Ulleung Interplane Gap between November 2002 and April 2004.

flows are considerably stronger than the southward flows, but they are confined to a narrower area near Dokdo as compared to the width of the southward flow. It can be seen that when the southward flow becomes stronger at EC1, the northward flows at KT and ET are also strengthened. When the deep flow at EC1 was directed to the north in December 2002, February, September, and December 2003, southward flows occurred at KT and ET or the northward flows became weakened, indicative of the negative correlation between the southward and northward flows. Fluctuations of deep currents at KT are concomitant with those at ET except for the period in September 2003 when the flow directions at two moorings were opposite. The record-length mean volume transport based on the data from five moorings is negligibly small, but the range of the transport fluctuations is large from -1.0 Sv (southward) to 0.7 Sv (northward). More details on the transport fluctuations will be analyzed and published elsewhere.

6. SST and Remote Sensing

To understand the dynamics of various oceanographic processes in the East Sea, it is essential to collect as much time series data as possible using the methodology described earlier. However, it is very difficult and expensive to produce time series data with a fairly good spatial resolution under diverse atmospheric and oceanic conditions. It is much more difficult to conduct a cruise in winter rather than summer due to the severe weather conditions, especially in the northern part of the East Sea. Remotely-sensed synoptic satellite data may provide us with valuable information even though the data is mostly limited to the sea surface. Since many of satellite programs have been conducted by NASA (National Aeronautics and Space Administration) or ESA (European Space Agency) to understand global changes in climate and ocean, most algorithms for geophysical parameter retrievals have focused on gross variation on a global scale. This discrepancy in spatial scales may generate unexpected errors in applying global coefficients to the regional seas like the East Sea. During the past decade, we have tried to derive reliable estimates of satellite-derived parameters to meet the scientific research requirements for the oceanic features in the East Sea such as eddies, fronts, currents, and basin-

wide circulation. Out of many satellite-derived oceanic variables, here we briefly introduce our endeavors to validate and optimize the satellite data to the East Sea, *e.g.*, SST data from NOAA/AVHRR (National Oceanic and Atmospheric Administration/Advanced Very High Resolution Radiometer), satellite scatterometer-derived wind vectors from NSCAT (NASA Scatterometer) and QuikSCAT, and altimetric data from TOPEX/Poseidon. We also briefly introduce some of applications utilizing such data.

Regional bias and optimization of sea surface temperature

SNU/RIO (Research Institute of Oceanography) has been receiving NOAA/HRPT (High ransmission) data at SNU station since 1989 and at ESOREC (East Sea Ocean Research Center of RIO) station since 1999. Among the many possible equations to derive SST from AVHRR data, SNU/RIO has used the most commonly-used split-window MCSST (Multi-Channel Sea Surface Temperature) equations of NOAA/NESDIS (National Environmental Satellite, Data, and Information Service). Park *et al.* (1999) compared satellite-derived SSTs with temperatures measured by thirty-four satellite-tracked ARGOS drifters deployed in the East Sea from 1993 to 1997. As a result, the split window technique showed relatively small rms errors in the range of 0.9°C to 1.2°C compared with other window methods. However, it tends to estimate satellite-based SSTs lower than *in situ* measurements by greater than 2°C, particularly in winter when the atmosphere over the sea surface is very dry and the seawater temperature is relatively low. On the other hand, satellite-derived SST estimates are higher than *in situ* temperatures under moist atmospheric conditions in summer. This tendency toward underestimation in winter may bring about serious errors in the study of the cold water formation in the East Sea, which is a critical issue involved in understanding the circulation of the East Sea. In order to reduce the errors resulting in the underestimation or overestimation of satellite-based SSTs, the new coefficients of the equations were optimized to the specific conditions of the regional sea. As a result, the characteristic trend could be removed and its associated rms errors for the new SST equations could be reduced to 0.3°C~0.9°C. SST estimates based on the global database can be successfully utilized over a medium range of temperatures, but in the case of extremely low temperatures, satellite-derived SST based on global coefficients fails to reproduce absolute values, although it can reveal the spatial structures of oceanic features. To give an example of regional problems in using the global algorithm, Fig. 16a demonstrates that unreasonably low temperatures of less than 0°C, close to -2°C in some areas, are found over a wide area in the northern East Sea. This problem was overcome by optimizing the SST coefficients in the regional sea as shown in Fig. 16b.

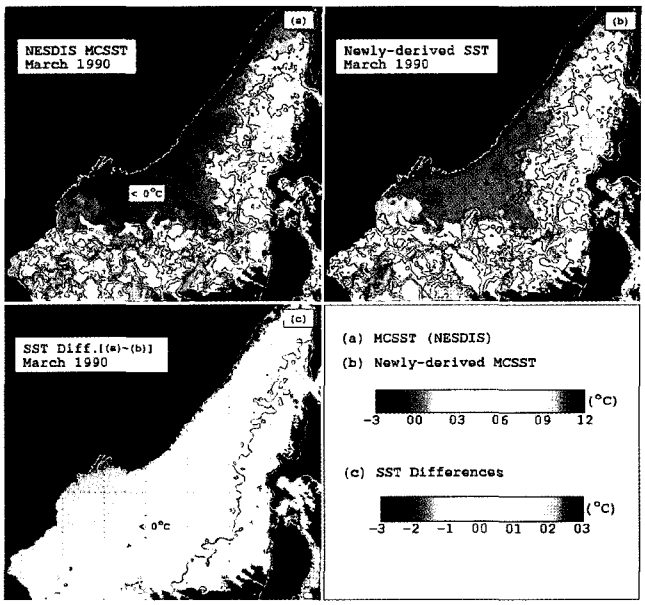

Fig. 16. Comparison of SSTs estimated from (a) NOAA/NESDIS algorithm, (b) regionally-optimized SST equations, and (c) their differences, (a)-(b) (Park *et al.* 1999)

The temperature difference between the two, however, is as large as -2°C in some areas. More fundamentally, these characteristic errors of satellite-derived SSTs might be associated with the differences between bulk temperature and surface skin temperature (Park *et al.* 1994), which should be further elucidated.

Regional bias of satellite scatterometer-observed wind vectors

A satellite scatterometer is a microwave radar sensor used to measure the backscattering at the sea surface. This instrument transmits radar pulses to the sea surface and measures the radar energy reflected back towards the source. Changes in sea surface roughness, which arises from changes in wind velocity, affect backscattered power. This gives us information of sea surface wind speed. Directions of wind vectors are acquired by multiple, collocated, and nearly simultaneous measurements by satellite antennas. Since scatterometer winds are highly indirectly derived from the backscattering cross section at the sea surface, 10-m neutral winds by applying a geophysical model function are substantially different from real winds measured at buoys.

To validate satellite scatterometer-observed wind vectors and understand error characteristics, both NSCAT and QuikSCAT/SeaWinds wind vectors are collocated with wind measurements at three JMA (Japanese Meteorological Agency) buoys in the East Sea, the East China Sea, and south of Japan within a gap of 30 minutes in time and

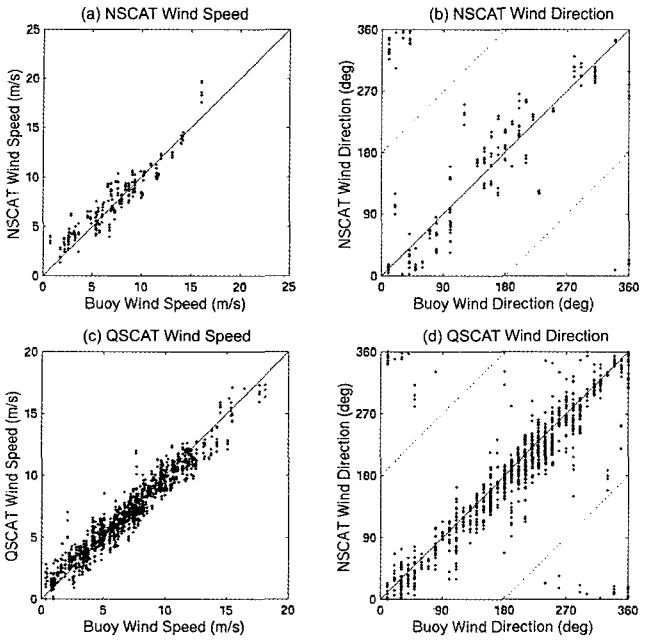

Fig. 17. Comparison of satellite-derived winds with in-situ winds from three JMA buoys in the seas adjacent to Korea: (a) NSCAT wind speed, (b) NSCAT wind direction, (c) QuikSCAT wind speed, and (d) QuikSCAT wind direction.

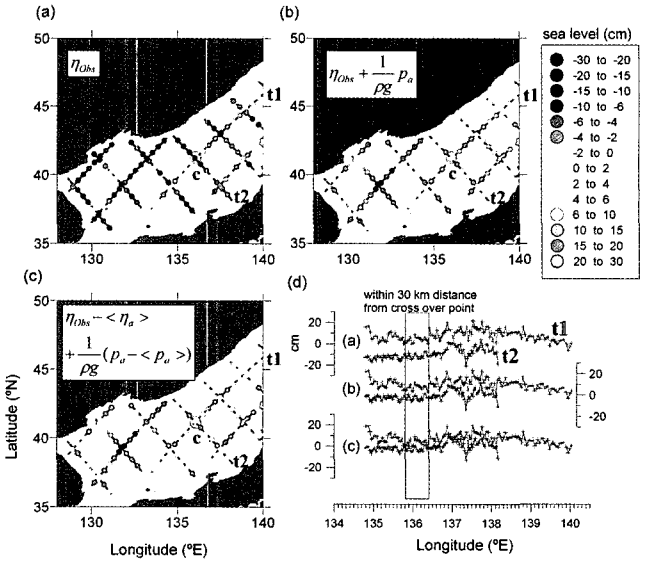

Fig. 18. T/P track data for ten days with (a) no correction, (b) IB correction, (c) correction for non-isostatic sea level response, and (d) sea surface height anomaly along two crossing tracks (t1 and t2) (Nam *et al.* 2004a).

25 km in space (Fig. 17). Buoy winds measured at 7.5 m are converted to near-surface winds of 10 m based on the LKB model (Liu *et al.* 1979). All wind records during the NSCAT period (September 1996~June 1997) and QuikSCAT winds (July~December 1999) were used in the matching procedure. Wind vectors with poor quality and rain flag were all eliminated. RMS errors of the scatterometer wind speeds are relatively small with a range of 0.9~1.3 m s^{-1}, which meets the requirement of the scatterometer mission of 2 m s^{-1}. However, wind directions show a large scatter with rms errors from 15~40 degrees (Park *et al.* 2003), which may arise from ambiguity removal errors as well as random and systematic errors particularly at low wind vectors, and also geophysical model function uncertainty (Freilich 1997). The regional biases for wind vectors in the East Sea were exceedingly large compared to those reported values. The errors show a significant systematic bias, which depend on wind speed and atmospheric stability in the marine boundary layer (MBL). These regional biases and error characteristics of satellite scatterometer-observed winds in the East Sea with respect to atmospheric stability, MBL dynamics, or sea surface currents (Cornillon and Park 2001; Park and Cornillon 2002) will be reported in other papers.

Sea surface height from satellite altimetry

We have also optimized TOPEX/Poseidon altimeteric data by applying a correction for nonisostatic sea level response to atmospheric pressure instead of standard inverse barometric correction (Nam et al. 2004a). The sea level response to atmospheric pressure is non-isostatic in the East Sea for periods shorter than a week due to a Helmholtz-like resonance between the East Sea and the Pacific through the straits (Lyu et al. 2002a). Because rms differences between standard inverse barometric (IB) correction and the non-isostatic response correction is 2~3 cm with a maximum difference of up to 10 cm, this non-isostatic response should be eliminated from the altimetry data to investigate ocean circulation and its variability relevant to the subsurface motions in the East Sea (Fig. 18). It causes the 'trackiness' errors between the neighboring tracks and aliasing effects in the altimetry data. The sea level differences between the two tracks (t1 and t2) which is averaged within 30 km from the crossover point (labeled c in (a), (b), and (c)), are 15.3, 9.7, and 6.2 cm in (a), (b), and (c) respectively. The best reduction was obtained by applying a correction for nonisostatic sea level response to atmospheric pressure instead of a standard inverse barometric correction. Therefore, we eliminated the pressure-driven high-frequency fluctuations in the TOPEX/Poseidon altimetric data, applying the simple analytic model suggested by Lyu et al. (2002a) (Nam et al. 2004a).

Some applications

Multi-satellite data enable us to make a variety of oceanic applications. Based on the SST database over a decade, we first presented a new spatial structure of SST

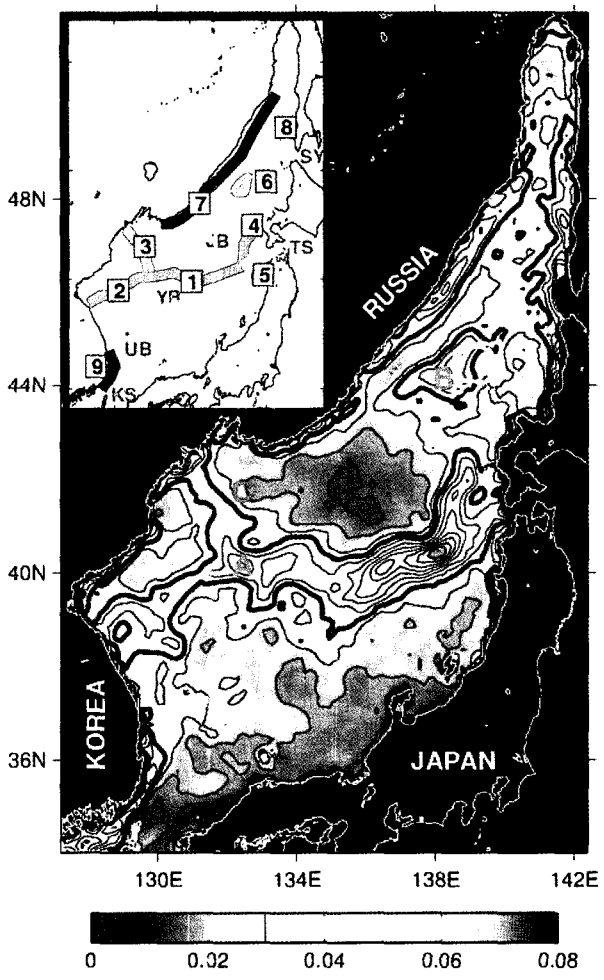

Fig. 19. SST fronts in the East Sea (Park *et al.* 2004a).

fronts based on a long-term averaged frontal map of the entire East Sea (Fig. 19). Fronts in the East Sea can be assigned to the Subpolar Front (SPF) in its central sea areas and to other fronts along the continental shelves (Park *et al.* 2004a). The SPF is located mostly along about 40°N between 132.3°E and 138°E, but bifurcates at both its eastern and western ends with strong seasonality. The SPF bifurcates into its northwestern branch (NWSPF) and the front around a warm eddy off the east coast of Korea at its western side. We have shown that the NWSPF is developed by differential surface cooling in downwind and off-wind areas due to strong air-sea interaction in late autumn and winter. The eastern end of the SPF also shows conspicuous bifurcation in the vicinity of the Tsugaru Strait. We also found unreported fronts around a seamount in the northeastern area of the JB. The faster response to strong winds of the shallow water column overlying the seamount is thought to be responsible for a large SST gradient along the periphery of the seamount.

In addition, we have monitored spatial and temporal variations of SST using various kinds of infrared data. Satellite-observed SST data demonstrated that the annual cycle of SST north of the SPF was characterized by relatively large amplitude and variance, and earlier cooling as compared to those south of the SPF. We could also monitor when and where surface cooling reaches a peak in the entire area of the East Sea. It is noted that a particularly noticeable feature in the annual phase of earlier cooling was found over the seamount south of Vladivostok. This implies that bottom topography of the seamount plays a significant role in the cooling process after stratification breaks down in winter (Park *et al.* 2004d). Spatial distributions of the satellite-derived annual SST signal along with the time of maximum surface cooling are of importance in understanding where the formation of intermediate and deep waters in the East Sea in winter.

As one of the characteristics of the East Sea similar to that of the open ocean, there is sea ice in Peter the Great Bay and in the Tatarsky Strait. Spatial distribution and temporal variation of sea ice can be monitored using multi-satellite data. In addition, we have utilized satellite scatterometer-observed wind vectors (SSM/I, NSCAT and QuikSCAT) to understand atmospheric wind forcing (Park *et al.* 2003) and impact of wind forcing on nutrients, to investigate chlorophyll distribution from SeaWiFS data and biogeochemical environment (Park *et al.* 2004b), and to estimate the air-sea gas exchange coefficient (Park *et al.* 2004c).

7. Concluding Remarks

Out of our diverse activities for long-term measurements of water properties, currents, and circulation in the East Sea, we have briefly introduced a history of development and a monitoring system currently in operation: monitoring volume transport through cable voltage measurement across the Korea Strait, monitoring vertical profiles of temperature and salinity of water mass from upper to intermediate depths over the entire East Sea using ARGO floats, monitoring time series variations of oceanic and atmospheric variables using the ESROB system, a current meter mooring system to monitor deep currents, and a synoptic satellite observing system.

Each monitoring system has been implemented owing to remarkable technical advances in data communication methods, highly accurate instruments of CTD and ADCP, fast progress in satellite sensor development, a new type of profiling of ARGO floats for intermediate and deep layers. Since all of our monitoring systems are unmanned and on a real-time basis except for current moorings, we can obtain a bunch of oceanic measurements in laboratories almost at almost near real-time through diverse communication

systems based on cellular phone communication, fast Internet connection, or satellite communication systems. These data sets allow us to conduct research more synthetically in terms of space and time.

Much of the data from our monitoring system show multi-scale temporal variability from tens of seconds to over a decade. Utilizing those data combined with shipboard measurements, we can understand a wide range of spatial and temporal variability in the oceanic features of the East Sea. Regular surveys once or twice a year have been made along a meridional line from the coast of Russia to the UB since 1993. Water masses were newly classified (Kim *et al.* 2004a), and wintertime renewal of bottom water was observed (Kim *et al.* 2002). However, we have not much knowledge yet on the timing and location of water mass formation and associated deep circulation outflows through the Tsugaru and Soya Straits, or on the dynamics of upper circulation variability. To better understand those features and to establish an operational prediction system, it is necessary to construct a more comprehensive monitoring system with better coverage in space and time and utilize the most advanced instrumentation and techniques.

We have deployed ARGO floats in the East Sea as well as in the Northwest Pacific Ocean under the national ARGO program. As ARGO floats provide unprecedented data for diverse applications on water mass, deep current, inertial energy, not only in the East Sea, but also in the global ocean, attempts are being made to augment the number of floats deployed. For the circulation in shallow regions, we will be able to devise a shallow-water ARGO float with a parking depth of about a few hundred meters. Moored buoys need to be installed at other coastal regions to monitor and understand coastal processes, especially to monitor the variability of southward flowing North Korean Cold Currents together with the northward flowing East Korean Warm Currents. We plan to investigate further the characteristics and dynamics of identified high-frequency waves with more monitoring buoys.

We have also been successfully monitoring deep flows using current meter moorings on a delayed-mode basis, but the mooring activity is currently limited to the southwestern East Sea in the UIG. Variability of observed deep currents in the UIG and its linkage to deep flows in the JB, where the formation of subsurface water masses occur, are yet to be understood. We plan to deploy and maintain new current moorings in the JB and additional moorings in the UB, which will contribute to our understanding of deep circulation and variability in the East Sea.

One of the most admirable leaps in oceanic observations, which have been conducted over the past half-century, concerns the use of satellites and their various ocean sensors. Despite its limitations in observing the sea surface only, many satellites have been launched and transmit a huge amount of synoptic real-time information. These remote-sensing data give us unlimited potential applications in studying various features occurring in the East Sea. The platforms send their observations to the earth stations as long as they are in operation. Moreover, there are many existing and upcoming worldwide programs for observing the Earth to cope with abrupt and unexpected changes due to global warming and anthropogenic destruction of nature. As a tool of observing the earth, a vast amount of satellite remote sensing data stimulates us to establish future plans to expand our satellite data acquisition systems with better equipment than now. SNU/RIO plans to receive as much satellite data as possible by installing the acquisition systems. Synthetic, synoptic, simultaneous, and repeated satellite observations will undoubtedly elevate our knowledge of the East Sea.

As was stated earlier, just only a decade has passed since we inaugurated in-situ measurements of currents and water properties in the East Sea. Despite our relatively short observation history, we have made lots of new findings. But still, there are many unresolved oceanographic issues in the East Sea. These lead us to promote, thorough construction of the 4-D long-term, real-time monitoring system, operational oceanography for ascertaining present conditions and forecasting conditions on the East Sea in the near future.

Acknowledgements

This research was supported by the Brain Korea 21 Project through the School of Earth and Environmental Science, Seoul National University. This study was carried out as a part of "A Study on the Monitoring of the Global Ocean Variability with ARGO Program" supported by the Meteorological Research Institute/KMA. This study was supported by the Ministry of Environment as "The Eco-technopia 21 project" and also supported in part by the Agency for Defense Development and the Ministry of Science and Technology, Korea through Underwater Acoustics Research Center (UA-11) program (UD970022AD), National Research Laboratory (NRL) program: Real-time Monitoring of Ocean Environmental Change (2000-N-NL-01-C-012), and KORDI's in-house Project (PE87000).

References

Chang, K.-I., Y.-B. Kim, M.-S. Suk, and S.-K. Byun. 2002a. Hydrography around Dokdo. *Ocean and Polar Res.*, **24**, 369-389.

Chang, K.-I., N.G. Hogg, M.-S. Suk, S.-K. Byun, Y.-G. Kim, and K. Kim. 2002b. Mean flow and variability in the southwestern East Sea. *Deep-Sea Res. Part I*, **49**, 2261-2279.

Chang, K.-I., W.J. Teague, S.J. Lyu, H.T. Perkins, D.-K. Lee, D.R. Watts, Y.-B. Kim, D.A. Mitchell, C.M. Lee, and K. Kim. 2004. Circulation and currents in the southwestern East/Japan Sea: Overview and review. *Prog. Oceanogr.*, **61**, 105-156.

Cornillon, P. C. and K.-A. Park. 2001. Warm core ring velocity inferred from NSCAT. *Geophys. Res. Lett.*, **28**, 575-578.

Csanady, G. T. 1984. Circulation in the coastal ocean. D. Reidel Publishing Co., Holland.

Freilich, M. H. 1997. Validation of vector magnitude datasets: effects of random component errors. *J. Atmos. Oceanic. Tech.*, **14**, 695-703.

Hogan, P. J. and H. E. Hullbert. 2000. Impact of upper ocean-topographical coupling and isopycnal outcropping in Japan/ East Sea models with 1/8° to 1/64° resolution. *J. Phys. Oceanogr.*, **30**, 2535-2561.

Holloway, G., T. Sou, and M. Eby. 1995. Dynamics of circulation of the Japan Sea. *J. Mar. Res.*, **53**, 539-569.

Kim, C. H. and K. Kim. 1983. Characteristics and origin of the cold water mass along the east coast of Korea. *J. Korean Soc. Oceanogr.*, **18**(1), 73-83.

Kim, C.-H. and J.-H. Yoon. 1999. A numerical modeling of the upper and the intermediate layer circulation in the East Sea. *J. Oceanogr.*, **55**, 327-345.

Kim, D.-J, W.M. Moon, S.H. Nam, and K. Kim. 2003. Evaluation of ENVISAT ASAR data for measurement of surface wind field over the Korean east coast. *Proc. IGARSS* 2003.

Kim, H. R., S. Ahn, and K. Kim. 2001. Observations of highly nonlinear internal solitons generated by near-inertial internal waves off the east coast of Korea. *Geophys. Res. Lett.*, **28**(16), 3191-3194.

Kim, K., K.-R. Kim, Y.-G. Kim, Y.-K. Cho, J.-Y. Chung, B.-H. Choi, S.-K. Byun, G.-H. Hong, M. Takematsu, J.-H. Yoon, Y. Volkov, and M. Danchenkov. 1996. New findings from CREAMS observations: Water masses and eddies in the East Sea. *J. Korean Soc. Oceanogr.*, **31**, 155-163.

Kim, K., Y. G. Kim, K.-W. Kim, and H. Ossi. 1999. Real-time ocean buoy off the east coast of Korea. p. 1-6. In: *Proc. Int. Sym. Prog. Coastal Eng. Oceanogr.* Seoul, Korea.

Kim, K., K.-R. Kim, D.-H. Min, Y. Volkov, J.-H. Yoon, and M. Takematsu. 2001. Warming and structural changes in the East (Japan) Sea: a clue to future changes in global oceans ? *Geophys. Res. Lett.*, **28**(17), 3293-3296.

Kim, K., K.-R. Kim, Y.-G. Kim, Y.-K. Cho, D.-J. Kang, M. Takematsu, and Y. Volkov. 2004a. Water masses and decadal variability in the East Sea (Sea of Japan). *Prog. Oceangr.*, **61**, 157-174.

Kim, K., S. J. Lyu, Y. -G. Kim, B. H. Choi, K. Taira, H. T. Perkins, W. J. Teague, and J. W. Book. 2004b. Monitoring Volume Transport through Measurement of Cable Voltage across the Korea Strait. *J. Atmos. Ocean. Tec.*, **21**, 671-682.

Kim, K., S. H. Nam, D. -J. Kim, K.-W. Kim, H. Ossi, Y.-G. Kim, and J.-W. Seo. 2004c. Real-time wave measurement using an ocean monitoring buoy. p. 83-92. In: *Workshop on wave, tide observation and modeling in the Asian-Pacific Region.*

Kim, Y.-G. and K. Kim. 1999. Intermediate Waters in the East/ Japan Sea. *J. Oceanogr.*, **55**, 123-132.

Kim, Y.-G., K. Kim, Y.-K. Cho, and H. Ossi. 2000. CTD data processing for CREAMS expeditions: Thermal-lag correction of Sea-Bird CTD. *J. Korean Soc. Oceanogr.*, **35**(4), 192-199.

Kobayashi T, Y. Ichikawa, Y. Takatsuki, T. Suga, N. Iwasaka, K. Ando, K. Mizuno, N. Shikama, and K. Takeuchi. 2001. Quality control of ARGO data based on high quality climatological dataset (HydroBase). I. ARGO Technical Report, FY2001, 36-48.

Larsen, J. C. 1992. Transport and heat flux of the Florida Current at 27°N derived from cross-stream voltages and profiling data: theory and observations. *Philos. Trans. R. Soc. London*, **A338**, 169-236.

Larsen, J. C., R. L. Mackie, A. Manzella, A. Fiordelisi, and S. Rieven. 1996. Robust smooth magnetotelluric transfer functions. *Geophys. J. Int.*, **124**, 801-809.

Liu, W.T, K.B. Katsaros, and J.A. Businger. 1979. Bulk parameterization of the air-sea exchange of heat and water vapor including the molecular constraints at the interface. *J. Atmos. Sci.*, **36**, 1722-1735.

Lyu, S. J. and K. Kim. 2003. Absolute transport from the sea level difference across the Korea Strait. *Geophys. Res. Lett.*, **30**, 1285, doi:10.1029/2002GL016233.

Lyu, S. J., K. Kim, and H. T. Perkins. 2002a. Atmospheric pressure-forced subinertial variations in the transport through the Korea Strait. *Geophys. Res. Lett.*, **29**, 1294, doi:10.1029/2001GL014366.

Lyu, S. J., Y.-G. Kim, K. Kim, J. W. Book, and B. H. Choi. 2002b. Tidal variations in the cable voltage across the Korea Strait. *J. Korean Soc. Oceanogr.*, **37**, 1-9.

Nam, S. H., K.-W. Kim, H. R. Kim, C. B. Cho, S. J. Lyu, Y. G. Kim, and K. Kim. 2003. Development of ESROB (East Sea Real-time Ocean Buoy). In: *PICES Scientific Report series from 2002 MONITOR workshop,* Qingdao, China.

Nam, S. H., S. J. Lyu, Y. H. Kim, K. Kim, J.-H. Park, and D. R. Watts. 2004a. Correction of TOPEX/POSEIDON altimeter data for nonisostatic sea level response to atmospheric pressure in the Japan/East Sea. *Geophys. Res. Lett.*, **31**(2), L02304, doi: 10.1029/2003GL018487.

Nam, S. H., J. Y. Yun, and K. Kim, 2004b. Observations on the coastal ocean response to typhoon 'Maemi' at the East Sea Real-time Ocean Buoy. *J. Korean Soc. Oceanogr. (The Sea)*, **9**(3), 111-119.

Nam, S. H., Y. H. Kim, K.-A. Park, and K. Kim. 2004c. Spatio-temporal variability in sea surface wind stress near and off the east coast of Korea. *Acta. Oceanol. Sin.*, **24**(1). (In press)

Park, J.J., K. Kim, J.-C. Nam, Y.-H. Youn, H.M. Lee, and J.-W. Seo. 2002. Data validation from ARGO float. *Proc. Korean Meteorol. Soc.* Spring, Seoul, Korea.

Park, J.J. and K. Kim. 2003. Importance of surface water property in previous winter on the formation of HSIW in the East/Japan Sea. *PICES*, Seoul, Korea.

Park, J.J., K. Kim, and W. R. Crawford. 2004. Inertial currents estimated from surface trajectories of ARGO floats. *Geophys. Res. Lett.*, **31**, L13307, doi:10.1029/2004GL020191.

Park, J.J., K. Kim, B. A. King, and S. C. Riser. 2005. An advanced method to estimate deep current from ARGO floats. *J.*

Atmos. Oceanic Tech. (In press).

Park, J.J., K. Kim, and B. A. King. 2005. Global Statistics of inertial motions. *Gephys. Res. Lett.* (In preparation).

Park, K.-A., J. Y. Chung, K. Kim, and B. H. Choi. 1994. A study on comparison of satellite drifter temperature with satellite derived sea surface temperature of NOAA/NESDIS. *J. Korean Soc. Remote Sensing*, **11**(2), 83-107.

Park, K.-A., J. Y. Chung, K. Kim, B. H. Choi, and D. K. Lee. 1999. Sea surface temperature retrievals optimized to the East Sea (Sea of Japan) using NOAA/AVHRR data. *Marine Technol. Soc. J.*, **33**(1), 23-35.

Park, K.-A. and P. C. Cornillon. 2002. Stability-induced modification of sea surface winds over Gulf Stream rings. *Geophys. Res. Lett.*, **29**(24), 2211-2214.

Park, K.-A., K. R. Kim, K. Kim, J. Y. Chung, and P. C. Cornillon. 2003. Comparison of wind speed from an atmospheric pressure map (Na wind) and satellite scatterometer-observed wind speed (NSCAT) over the East (Japan) Sea. *J. Korean Soc. Oceanogr.*, **38**(4), 173-184.

Park, K.-A., K. Kim, K.R. Kim, J.Y. Chung, and P. C. Cornillon. 2003. Spatial and temporal variability of sea surface winds and Ekman pumping retrieved from satellite scatterometer-observed wind vectors over the East Sea. In: *PICES*, Seoul, Korea.

Park, K.-A., J. Y. Chung, and K. Kim. 2004a. Sea surface temperature Fronts in the East (Japan) Sea and temporal variations. *Geophys. Res. Lett.*, **31**, L07304, doi:10.1029/2004GL019424.

Park, K.-A., K. Kim, K. R. Kim, P.C. Cornillon, and C.-O. Jo. 2004b. Ekman pumping variability in the East (Japan) Sea and its impact on nutrient distributions. In: *6th IOC/WESTPAC Symposium*, Hangzhou, China.

Park, K.-A., J. Y. Chung, and K. R. Kim. 2004c. SST Applications at SNU/RIO. In: *6th IOC/WESTPAC Symposium*, Hangzhou, China.

Park, K.-A., J. Y. Chung, K. Kim, and P. C. Cornillon. 2004d. Wind and bathymetric forcing of the annual sea surface temperature signal in the East (Japan) Sea. *Geophys. Res. Lett.*, 32, L5610, doi:10. 1029/2004GL022197.

Park, Y.-G, K.-H. Oh, K.-I. Chang, and M.-S. Suk. 2004. Intermediate level circulation of the southwestern part of the East/Japan Sea estimated from autonomous isobaric profiling floats. *Geophys. Res. Lett.*, **31**, L13213, doi:10.1029/2004GL020424.

Sanford, T. B. and R. E. Flick. 1975. On the relationship between transport and motional electric potentials in broad, shallow currents. *J. Mar. Res.*, **33**, 123-139.

Takikawa, T., J.-H. Yoon, H. Hase, and K.-D. Cho. 1999. Monitoring of the Tsushima Current at the Tsushima/Korea Straits. p. 15-18. In: *Proc. 3rd CREAMS Int. Symp.*, Fukuoka, Japan. Japanese Ministry of Education, Science, Sports and Culture.

Teague, W. J., G. A. Jacobs, H. T. Perkins, J. W. Book, K.-I. Chang, and M.-S. Suk. 2002. Low-frequency current observations in the Korea/Tsushima Strait. *J. Phys. Oceanogr.*, **32**, 1621-1641.

Teague, W.J., K.L. Tracey, D.R. Watts, J.W. Book, K.-I. Chang, P.J. Hogan, D.A. Mitchell, M.-S. Suk, M. Wimbush, and J.-H. Yoon. 2005. Observed deep circulation in the Ulleung Basin. *Deep-Sea Res. II.* (In press)

Wong, A. P. S., G. C. Johnson, and W. B. Owens. 2003. Delayed-mode calibration of autonomous CTD profiling float salinity data by theta-S climatology. *J. Atmos. Oceanic Tech.*, **20**, 308-318.